Nematic order in a simple-cubic lattice-spin model with full-ranged dipolar interactions

Hassan Chamati[1,*] and Silvano Romano[2,†]
[1]*Institute of Solid State Physics, Bulgarian Academy of Sciences, 72 Tzarigradsko Chaussée, 1784 Sofia, Bulgaria*
[2]*Physics Department, The University, via A. Bassi 6, 27100 Pavia, Italy*
(Received 31 January 2016; published 31 May 2016)

In a previous paper [Phys. Rev. E **90**, 022506 (2014)], we studied the thermodynamic and structural properties of a three-dimensional simple-cubic lattice model with dipolarlike interaction, truncated at nearest-neighbor separation, for which the existence of an ordering transition at finite temperature had been proven mathematically; here we extend our investigation, addressing the full-ranged counterpart of the model, for which the critical behavior had been investigated theoretically and experimentally. In addition, the existence of an ordering transition at finite temperature had been proven mathematically as well. Both models exhibited the same continuously degenerate ground-state configuration, possessing full orientational order with respect to a suitably defined staggered magnetization (polarization), but no nematic second-rank order; in both cases, thermal fluctuations remove the degeneracy, so that nematic order does set in at low but finite temperature via a mechanism of order by disorder. On the other hand, there were recognizable quantitative differences between the two models as for ground-state energy and critical exponent estimates; the latter were found to agree with early renormalization-group calculations and with experimental results.

DOI: 10.1103/PhysRevE.93.052147

I. INTRODUCTION

Long-range dipolar interactions [1] between magnetic moments are ubiquitous in experimentally studied magnetic systems, although they are often dominated by exchange couplings (for more details, see Refs. [2–5] and references therein), and, over the past few decades, a number of theoretical studies, based on renormalization-group techniques, have addressed interaction models containing both dipolar and short-range isotropic or anisotropic exchange interactions (see, e.g., Refs [2,6–11]); on the other hand, lattice models involving only the long-range dipolar term have also long been studied using various approaches, including spin-wave treatments and simulation (see, e.g., Refs. [12–19], and others quoted in the following). While the former references have dealt with the resulting critical behavior, including the crossover between the isotropic dipolar universality class (when the dipolar term is dominant) and the Heisenberg one (corresponding to nearest-neighbor exchange interactions only), the latter were *mostly* focused on the ground state of the magnetically ordered phase; in addition, a survey of relevant rigorous mathematical results can be found in [20]. In a previous paper [16], we studied the thermodynamic and structural properties of a three-dimensional lattice model with dipolarlike interaction, truncated at nearest-neighbor separation, for which the existence of an ordering transition at finite temperature had been proven mathematically [21]. It was found that the ground state is degenerate and the critical behavior of the model is consistent with the Heisenberg universality class; moreover, the model was found to exhibit a nematic order induced by thermal disorder; the study of an *isolated* cubic dipole cluster [17] was published shortly afterward by other authors, and the degeneracy of the ground state was found in that case as well.

Some similar studies have been published only recently in Refs. [18,19], and they have addressed the ground state of a model of pure dipolar interaction considering different types of lattices; the magnetic properties of the ground state were determined for each lattice structure.

Among the above studies, only Ref. [16], which investigated a pure dipolar model with interaction restricted to nearest-neighbor pairs of sites, considered the possibility of nematic ordering both in the ground state and at finite temperature. Here we continue to address the full-ranged counterpart of the model, for which mathematical results have been produced [20] as well; the treatment was based on reflection positivity [22], and it proved the existence of an ordering transition at finite temperature, as predicted by spin-wave theory.

The interaction model studied here has long-range tails expected to alter the critical behavior of its counterpart investigated in Ref. [16]. Our results show a downward shift of the critical temperature, and, in addition, they lead to different values of critical exponents, as well as critical amplitudes, thus pointing to a class of universality beyond the nearest-neighbor Heisenberg one. We are also revisiting and correcting an earlier and crude simulation study of the full-ranged model, carried out by one of us some 30 years ago [23,24].

The rest of our paper is organized as follows: In Sec. II, results for the ground state of interaction potential (1) are recalled; the simulation methodology is briefly discussed in Sec. III; simulation results and finite-size scaling analysis are used in Sec. IV to extract the critical behavior for the model under consideration; and the paper is concluded in Sec. V, where results are summarized.

II. INTERACTION MODEL AND GROUND STATE

In keeping with our previous work [16,25], we are considering a classical system consisting of n-component magnetic moments to be denoted by unit vectors $\{\mathbf{u}_j\}$, with orthogonal Cartesian components $u_{j,\iota}$, defined with respect to lattice axes,

*chamati@bas.bg
†silvano.romano@pv.infn.it

associated with a d-dimensional lattice $\mathbb{Z}^d$ (here $d = n = 3$), and interacting via a translationally invariant pair potential of the form

$$V_{ij} = \epsilon f(r)[-3(\mathbf{u}_i \cdot \hat{\mathbf{r}}_{ij})(\mathbf{u}_j \cdot \hat{\mathbf{r}}_{ij}) + \mathbf{u}_i \cdot \mathbf{u}_j], \tag{1}$$

with ϵ a positive quantity setting energy and temperature scales (i.e., energies will be expressed in units of ϵ, and temperatures defined by $T = k_B \mathcal{T}_K/\epsilon$, where $\mathcal{T}_K$ denotes the temperature in degrees Kelvin), and

$$\mathbf{r}_{ij} = \mathbf{x}_i - \mathbf{x}_j, \quad r = |\mathbf{r}_{ij}|, \quad \hat{\mathbf{r}}_{ij} = \frac{\mathbf{r}_{ij}}{r}, \quad f(r) > 0;$$

here $\mathbf{x}_j$ denotes dimensionless lattice site coordinates, and now $f(r) = r^{-3}$; in Ref. [16] the interaction was restricted to nearest-neighbor separations, i.e., $f(r) = 1$ for $r = 1$ and 0 otherwise.

Both the full-ranged and the nearest-neighbor counterpart possess the same continuously degenerate ground-state configuration (see also below); the ground-state energies (in units ϵ per particle) are $W_{\mathrm{GS}} = -4$ for the nearest-neighbor model [16,25] and $W_{\mathrm{GS}} = -2.676$ for the present full-ranged counterpart [12,16,25]. Extensive references to Luttinger-Tisza methodologies for ground-state calculation can also be found in [19].

For the sake of clarity and completeness, we recall here some properties of the continuously degenerate ground state for the three-dimensional case ($d = 3$), closely following the corresponding section in our previous paper [16]. Let lattice site coordinates be expressed as $\mathbf{x}_j = \mathbf{x}(h,k,l) = h\mathbf{e}_1 + k\mathbf{e}_2 + l\mathbf{e}_3$, $d = 3$, where $\mathbf{e}_\alpha$ denotes unit vectors along the lattice axes; here the subscript in h_j has been omitted for ease of notation; let also $\varrho_h = (-1)^h$, $\sigma_{hk} = \varrho_h\varrho_k$, $\tau_{hkl} = \varrho_h\varrho_k\varrho_l$; the ground state possesses continuous degeneracy, and the manifold of its possible configurations is defined by [12]

$$\mathbf{u}_j^0 = \mathbf{u}^0(h,k,l) = \sigma_{kl}N_1\mathbf{e}_1 + \sigma_{hl}N_2\mathbf{e}_2 + \sigma_{hk}N_3\mathbf{e}_3, \tag{2}$$

where

$$N_1 = \sin\Theta\cos\Phi, \tag{3a}$$
$$N_2 = \sin\Theta\sin\Phi, \tag{3b}$$
$$N_3 = \cos\Theta, \tag{3c}$$

and $0 \leqslant \Theta \leqslant \pi$, $0 \leqslant \Phi \leqslant 2\pi$; we also found it advisable to use the superscript 0 for various ground-state quantities. The above configuration will be denoted by $D(\Theta,\Phi)$.

Various structural quantities can be defined, some of which are found to be zero for all values of Θ and Φ, or to average to zero upon integration over the angles; for example, when $d = 3$,

$$\sum_{j\in\Delta}\mathbf{u}_j^0 = \mathbf{0}, \tag{4a}$$
$$\sum_{j\in\Delta}\rho_h\mathbf{u}_j^0 = \mathbf{0}, \quad \sum_{j\in\Delta}\rho_k\mathbf{u}_j^0 = \mathbf{0}, \quad \sum_{j\in\Delta}\rho_l\mathbf{u}_j^0 = \mathbf{0}, \tag{4b}$$
$$\sum_{j\in\Delta}\tau_{hkl}\mathbf{u}_j^0 = \mathbf{0}. \tag{4c}$$

Here Δ denotes the d-dimensional unit cell, and $\varrho = 2^d$ is the number of particles in it; other staggered magnetizations are not averaged to zero upon summing over the unit cell:

$$\mathbf{B}_1^0 = \sum_{j\in\Delta}\sigma_{kl}\mathbf{u}_j^0 = \varrho N_1\mathbf{e}_1, \tag{5a}$$
$$\mathbf{B}_2^0 = \sum_{j\in\Delta}\sigma_{hl}\mathbf{u}_j^0 = \varrho N_2\mathbf{e}_2, \tag{5b}$$
$$\mathbf{B}_3^0 = \sum_{j\in\Delta}\sigma_{hk}\mathbf{u}_j^0 = \varrho N_3\mathbf{e}_3; \tag{5c}$$

thus, bearing in mind the above formulas, for any unit vector $\mathbf{u}_j$ associated with the lattice site $\mathbf{x}_j$, one can define another unit vector $\mathbf{w}_j$ with Cartesian components $w_{j,\kappa}$ via

$$w_{j,1} = \sigma_{kl}u_{j,1}, \tag{6a}$$
$$w_{j,2} = \sigma_{hl}u_{j,2}, \tag{6b}$$
$$w_{j,3} = \sigma_{hk}u_{j,3}, \tag{6c}$$

and hence the staggered magnetization

$$\mathbf{C} = \sum_{j\in\Delta}\mathbf{w}_j; \tag{7}$$

when $\mathbf{u}_j = \mathbf{u}_j^0, j = 1,2,\ldots,8$, i.e., for the ground-state orientations, Eqs. (2) and (7) lead to

$$\mathbf{C}^0 = \sum_{j\in\Delta}\mathbf{w}_j^0 = \mathbf{B}_1^0 + \mathbf{B}_2^0 + \mathbf{B}_3^0 = \varrho(N_1\mathbf{e}_1 + N_2\mathbf{e}_2 + N_3\mathbf{e}_3); \tag{8}$$

in this case,

$$\mathbf{w}_j^0 = N_1\mathbf{e}_1 + N_2\mathbf{e}_2 + N_3\mathbf{e}_3, \quad j = 1,2,\ldots,8. \tag{9}$$

The ground-state order parameter is defined by

$$\frac{1}{\varrho}\sqrt{\mathbf{C}^0\cdot\mathbf{C}^0} = 1. \tag{10}$$

Equations (3), (8), and (9) show that in all $D(\Theta,\Phi)$ configurations, the vector $\mathbf{C}^0$ has the same modulus, and that each $D(\Theta,\Phi)$ defines its possible orientation, or, in other words, the ground state exhibits full order and continuous degeneracy with respect to the above $\mathbf{C}^0$ vector. Notice also that the above transformation from $\mathbf{u}_j$ to $\mathbf{w}_j$ unit vectors [Eq. (6)] can, and will, be used in the following for arbitrary configurations of unit vectors $\mathbf{u}_j$ to calculate $\mathbf{C}$ [Eqs. (7)] and related quantities.

As for nematic ordering in the ground state, for a generic configuration $D(\Theta,\Phi)$, the nematic second-rank ordering tensor Q^0 is defined by [26–28]

$$Q_{\iota\kappa}^0 = \frac{3}{2\varrho}\sum_{j\in\Delta}\left(u_{j,\iota}^0u_{j,\kappa}^0\right) - \frac{\delta_{\iota\kappa}}{2}; \tag{11}$$

the above tensor turns out to be diagonal, i.e.,

$$Q_{\iota\kappa}^0 = \delta_{\iota\kappa}q_\kappa, \quad q_\kappa = P_2(N_\kappa). \tag{12}$$

The eigenvalue with the largest magnitude (to be denoted by $\overline{q}$) ranges between $-\frac{1}{2}$ and $+1$, it defines the nematic second-rank order parameter, and its corresponding eigenvector defines the nematic director $\mathbf{n}$ [26–28].

Some specific configurations and their corresponding $\overline{q}$ quantities are

$$D_1 = D(0,\Phi),\forall\ \Phi, \quad \overline{q} = +1, \tag{13a}$$

$$D_2 = D\left(\frac{\pi}{2},\frac{\pi}{4}\right), \quad \overline{q} = -\frac{1}{2}, \tag{13b}$$

$$D_3 = D\left(\arccos\left(\frac{1}{\sqrt{3}}\right),\frac{\pi}{4}\right), \quad \overline{q} = 0; \tag{13c}$$

other equivalent cases can be obtained from Eqs. (13) by appropriate choices of the two angles, corresponding to a suitable relabeling of lattice axes; for example, there are six possible D_1-type configurations, corresponding to $\mathbf{u}^0(0,0,0)$ being oriented in opposite senses along a lattice axis [i.e., $\mathbf{u}^0(0,0,0) = \pm\mathbf{e}_\alpha$, $\alpha = 1,2,3$].

As for geometric aspects of Eq. (13), in D_1-type configurations, all unit vectors $\mathbf{u}_j^0$ are oriented along a lattice axis, with appropriate signs of the corresponding components, i.e., a spin sitting at a lattice site and, say, its vertical neighbors point in the same sense, its horizontal nearest neighbors point in the opposite way, and then its horizontal next-nearest neighbors point in the same way, etc., and here full nematic order is realized. On the other hand, in D_2-type configurations, all unit vectors $\mathbf{u}_j^0$ lie on a lattice plane, and their components along the corresponding axes are $(\pm\sqrt{2}/2, \pm\sqrt{2}/2)$, with the four combinations of signs, producing antinematic order; finally, in D_3-type configurations, the unit vectors $\mathbf{u}_j^0$ have components along lattice axes given by $(\pm\sqrt{3}/3, \pm\sqrt{3}/3, \pm\sqrt{3}/3)$, with all possible combinations of signs; in the latter case, magnetic order of the unit vectors $\mathbf{w}_j^0$ is accompanied by no nematic order; the three named ground-state configurations can be seen in Fig. 1 of Ref. [16]. Notice also that, upon integrating over the two angles, the three quantities q_κ are averaged to zero; in other words, the ground-state possesses ferromagnetic order with respect to the $\mathbf{C}^0$ vectors, but its degeneracy destroys overall nematic order.

According to available mathematical results [20,21], overall magnetic order (in terms of $\mathbf{C}$ vector) survives at suitably low but finite temperatures; on the other hand, different D configurations might be affected by fluctuations to different extents, possibly to the extreme situation in which only some of them are thermally selected ("survive"); this behavior, studied in a few cases after 1980, is known as ordering by disorder; see, e.g. Refs. [29–35].

Actually, our additional simulations, presented in Sec. IV, showed evidence of nematic order by disorder: it was observed that simulations starting at low temperature from different configurations $D(\Theta,\Phi)$ quickly resulted in configurations remaining close to the above D_1 type, i.e., the $\mathbf{C}$ vector remained aligned with a lattice axis; this caused the onset of second-rank nematic order, as shown by sizable values of the corresponding order parameters $\overline{P}_2$ and $\overline{P}_4$; in turn, the nematic director remained aligned with the above $\mathbf{C}$ vector (see the following sections); thus simulation results will suggest that, in the low-temperature regime, the above six D_1-type configurations correspond to pure Gibbs states.

III. COMPUTATIONAL ASPECTS

Calculations were carried out using periodic boundary conditions, and on samples consisting of $N = L^3$ particles, with $L = 10$, 12, 16, 20, and 24. Simulations, based on the standard METROPOLIS updating algorithm, were carried out in cascade, in order of increasing temperature T, starting at $T = 0.01$; equilibration runs took between 25 000 and 50 000 cycles (where one cycle corresponds to N attempted Monte Carlo steps), and production runs took between 500 000 and 2 000 000; the Ewald-Kornfeld method with tin-foil (conducting) boundary conditions was used for calculating configuration potential energy [15,36,37].

Individual attempts were carried out by first randomly selecting a lattice site, followed by a selection of a lattice axis, and finally carrying out a random rotation of the selected particle around it; this algorithm was introduced by Barker and Watts some time ago [36,38].

The Ewald-Kornfeld formulas for the potential energy of a given configuration of dipoles contain both a pairwise summation over the direct lattice (usually truncated by the nearest-image convention) and a sum over reciprocal-lattice vectors (whose number is independent of N), essentially based on single-particle terms [15,36,37]; evaluating the energy variation resulting from the attempted random rotation of a selected particle requires considering interactions with the remaining $(N-1)$ particles, as well as a sum over the named reciprocal-lattice vectors: additional tests had shown that the computational effort requested by our program for attempting some large number of cycles (the same for different values of N) scaled with N like a linear combination $(a_1 N + a_2 N^2)$.

As for calculated thermodynamic and structural properties, as well as finite-size scaling (FSS) analysis, we closely followed Ref. [16]; the procedure for characterizing nematic orientational order is also reported in the Appendix.

Calculated quantities include the potential energy U in units ϵ per particle, and configurational specific heat C_V/k_B; as in Ref. [16], we use $\mathbf{C}$ to denote the staggered magnetization vector of a configuration, $\mathbf{m}$ for the corresponding unit vector, M for mean staggered magnetization, and χ for the corresponding susceptibility [39,40].

We also calculated the fourth-order Binder cumulant U_L of the staggered magnetization [16], as well as second- and fourth-rank nematic order parameters $\overline{P}_2$ and $\overline{P}_4$ [26–28], by analyzing one configuration every cycle (see also the Appendix for their definitions); the fourth-order cumulant, also known as the Binder cumulant [41], is defined by

$$U_L = 1 - \frac{\langle(\mathbf{C}\cdot\mathbf{C})^2\rangle}{3\langle\mathbf{C}\cdot\mathbf{C}\rangle^2}. \tag{14}$$

Correlation between staggered magnetization and even-rank orientational order [16] was also investigated; for a given configuration, let $\mathbf{n}$ denote the nematic director [26–28], and let $\mathbf{m}$ be the unit vector defined by $\mathbf{C}$; thus we calculated the quantity

$$\phi = \langle|\mathbf{m}\cdot\mathbf{n}|\rangle, \tag{15}$$

where ϕ ranges between $\frac{1}{2}$ for random mutual orientation of the two unit vectors, and 1 when they are strictly parallel or antiparallel [16].

IV. RESULTS

Simulation estimates of the potential energy per spin (not shown here) were found to vary in a gradual and continuous fashion against temperature and seemed to be largely unaffected by sample size to within statistical errors ranging up to 0.5%. In addition, they exhibited a smooth change of slope at about $T \approx 0.65$. This change is reflected on the behavior of the specific heat, whose fluctuation results showed a recognizably size-dependent maximum around the same temperature; the height of the maximum increases, and the full width at half-maximum decreases as the system size increases (Fig. 1); this behavior seems to develop into a singularity in the infinite-sample limit.

As in our previous paper [16], and as anticipated in Sec. II, analysis of simulation results showed that, in the ordered region, the staggered magnetization vector **C** remains aligned to a lattice main axis: for example, at $T \leqslant 0.05$, the component of **m** largest in magnitude was found to be $\geqslant 0.95$. As mentioned in the Introduction, a spin-wave treatment predicts orientational order at finite temperature, and the prediction was later mathematically justified in [20]: the present simulation results are consistent with a spin-wave picture of low-temperature excitations.

Results for the mean staggered magnetization M, plotted in Fig. 2, were found to decrease with temperature at fixed sample size. For temperatures below 0.5, the data for different sample sizes practically coincide, while for larger temperatures the magnetization decreases significantly as the system size increases. The fluctuations of M versus temperature are investigated through the susceptibility χ, shown in Fig. 3. We observed a pronounced growth of this quantity with the system size at about $T = 0.65$. This is manifested by a significant increase in the maximum height, as well as a shrinking of the full width at half-maximum, suggesting that the susceptibility will show a singularity as the system size goes to infinity. This behavior is evidence of the onset of a second-order phase transition.

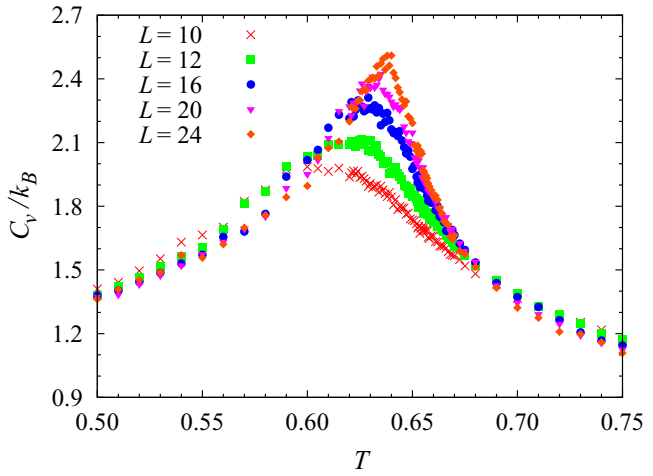

FIG. 1. Simulation results for the configurational specific heat, obtained with different sample sizes L; the statistical errors (not shown) range between 1% and 5%. Red crosses, $L = 10$; green squares, $L = 12$; blue circles, $L = 16$; magenta triangles, $L = 20$; and red diamonds, $L = 24$.

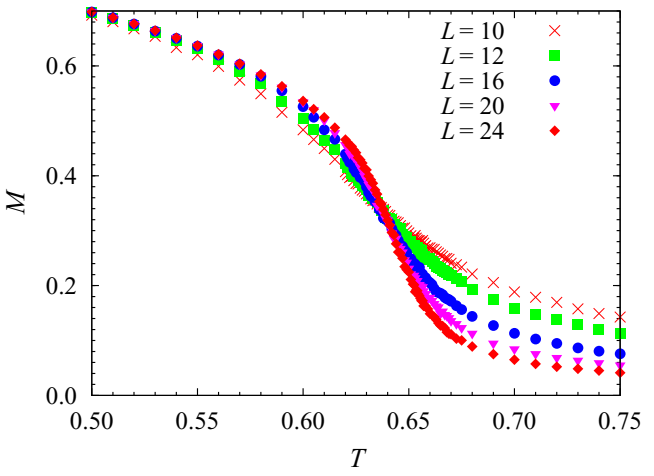

FIG. 2. Simulation estimates for the mean staggered magnetization M, obtained with different sample sizes; here and in the following figures, the errors fall within symbol size; same meaning of symbols as in Fig. 1.

To extract the critical behavior of our model, a detailed FSS analysis was applied first to the simulation data obtained for the staggered magnetization M (Fig. 2). This was an attempt to collapse all simulation measurements into a single curve describing the behavior of the corresponding scaling function according to the scaling law

$$M = L^{-\beta/\nu}\Theta_M(tL^{1/\nu}); \tag{16}$$

here $t = 1 - \frac{T}{T_c} \ll 1$ denotes the distance from the bulk critical temperature T_c, $\beta > 0$ is the critical exponent related to M in the bulk limit, i.e., $\lim_{L\to\infty} M \sim t^{\beta}$, and ν is the critical exponent for the correlation length ξ, i.e., $\xi \sim t^{-\nu}$; the function $\Theta_M(x)$ is a universal function depending on the gross features of the system, but not on its microscopic details.

To get the best estimates for the critical exponents, several attempts have been made on different sets of sample sizes following closely the procedure explained in Ref. [16], which

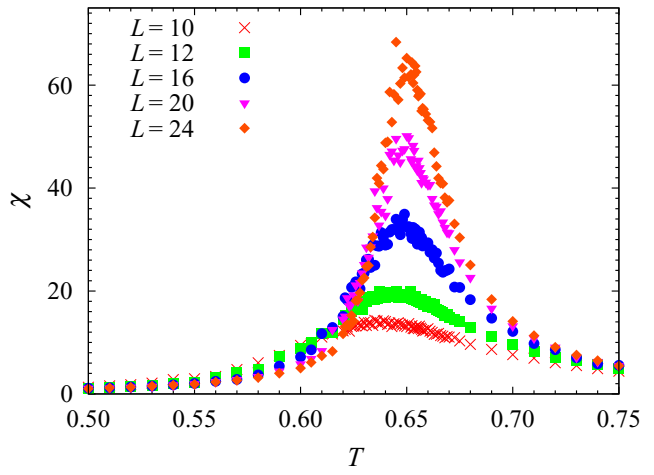

FIG. 3. Simulation estimates for the susceptibility χ associated with the staggered magnetization M, obtained with different sample sizes; same meaning of symbols as in Fig. 1.

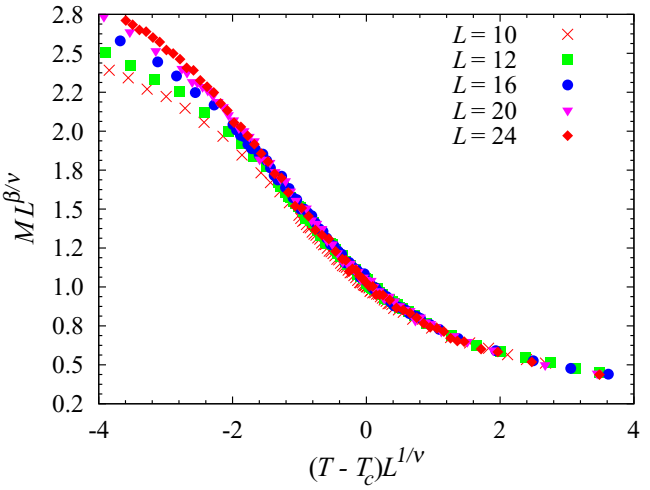

FIG. 4. Scaling behavior of the staggered magnetization M; same meaning of symbols as in Fig. 1.

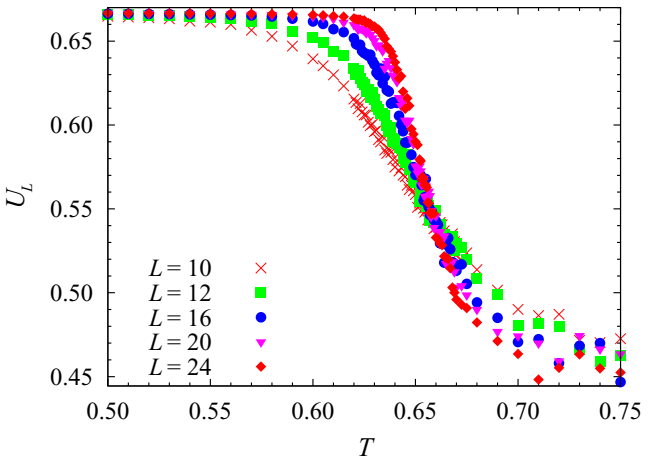

FIG. 5. Simulation results for the fourth-order Binder cumulant of the staggered magnetization [16] obtained with different sample sizes; same meaning of symbols as in Fig. 1.

is based on the minimization approach of Ref. [42]. The quality of the fit was controlled by a parameter S that was found to range between the values 1 and 2 for all quantities considered below. The behavior of the resulting scaling function for the staggered magnetization is reported in Fig. 4 with the critical temperature $T_c = 0.655 \pm 0.001$ and critical exponents $\beta = 0.38 \pm 0.03$ and $\nu = 0.69 \pm 0.03$.

A similar analysis was performed on the simulation data for the susceptibility χ leading to $T_c = 0.655 \pm 0.001$ and critical exponents $\gamma = 1.31 \pm 0.05$ and $\nu = 0.74 \pm 0.01$. Here we anticipate that, due to the large fluctuations of the susceptibility in the vicinity of the critical temperature (see, e.g., Fig. 3), this result may be incorrect. The fitting procedure was attempted on the specific heat as well, resulting in $T_c = 0.652 \pm 0.003$, $\alpha = 0.13 \pm 0.02$, and $\nu = 0.69 \pm 0.03$. These results indicate that accounting for the dipolar full-range interaction affects both nonuniversal quantities, such as the critical temperature, and universal features, i.e., critical exponents of various thermodynamic quantities. It is worth mentioning that a similar behavior is found in spin systems with algebraically decaying long-range interactions of ferromagnetic type (see, e.g., Ref. [43] and references therein also covering the bulk case).

Simulation estimates for the fourth-order Binder cumulant U_L are shown in Fig. 5. The plots for the different curves are found to decrease against the temperature and to intersect at about $T = 0.65$. A FSS of this quantity yields the critical temperature to a very good approximation, since a data collapse leads a scaling function that is independent on the sample size. This is found to be $T_c = 0.656 \pm 0.002$ and the critical exponent $\nu = 0.69 \pm 0.08$. At the critical temperature, we obtain the critical amplitude $U_L^* \approx 0.54$.

At all investigated temperatures, simulation results for the *nematic* order parameters $\overline{P}_2$ and $\overline{P}_4$ (Figs. 6 and 7) exhibited a gradual and monotonic decrease with temperature, vanishing above T_c, and they appeared to be mildly affected by sample sizes; results for $\overline{P}_4$ became negligible in the transition region, $T \gtrsim 0.55$ (not shown); in the low-temperature region, simulation results for both observables tended to saturate to 1 as $T \to 0^+$.

According to the FSS approach, the nematic order parameter is expected to scale like

$$\overline{P}_2 = L^{-2\beta/\nu}\,\Xi(tL^{1/\nu}). \tag{17}$$

Applying the above-mentioned minimization procedure, we get $T_c = 0.655 \pm 0.002$, $\beta = 0.37 \pm 0.02$, and $\nu = 0.69 \pm 0.03$, in very good agreement with the above finding for the staggered magnetization.

Simulation data for ϕ [Eq. (15)] are plotted in Fig. 8; for all investigated sample sizes, they appear to decrease with increasing temperature; moreover, the results exhibit a recognizable increase of ϕ with increasing sample size for $T \lesssim T_1 = 0.64$, and its recognizable decrease with increasing sample size for $T \gtrsim T_2 = 0.68$, so that the seemingly continuous change across the transition region becomes steeper and steeper as sample size increases. In the crossover temperature range between T_1 and T_2, the sample-size dependence of results becomes rather weak, and the various curves come close to coincidence at $T \approx 0.66 \pm 0.01$, with $\phi \approx 0.54$; notice that

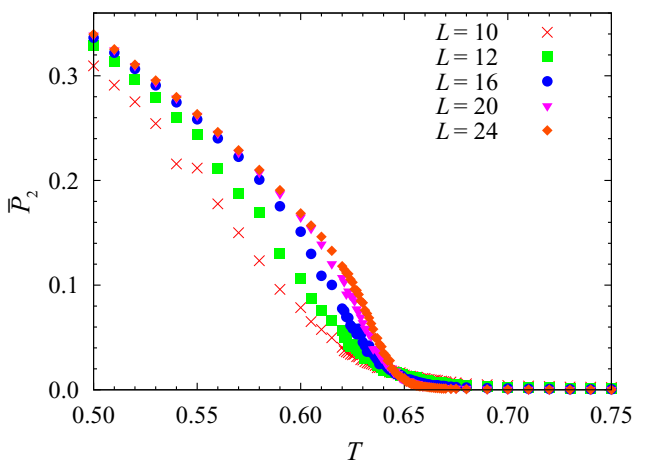

FIG. 6. Simulation results for the nematic second-rank order parameter $\overline{P}_2$, obtained with different sample sizes: same meaning of symbols as in Fig. 1.

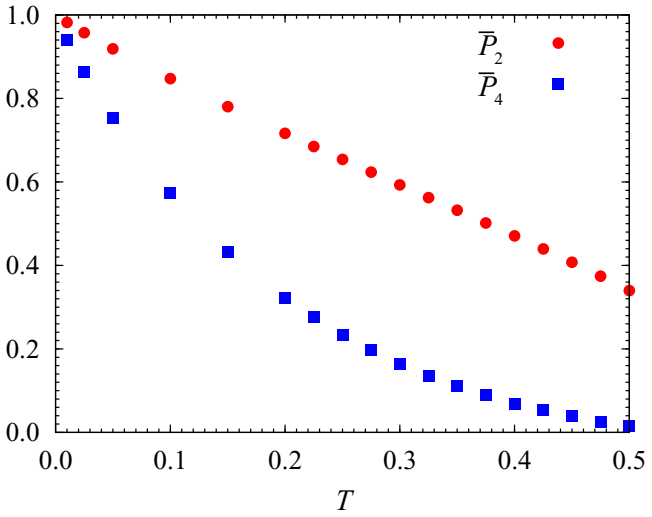

FIG. 7. Comparison between simulation results for nematic second- and fourth-rank order parameters, in the low-temperature region, and obtained with the largest investigated sample size $L = 24$. Red circles, $\overline{P}_2$; blue squares, $\overline{P}_4$.

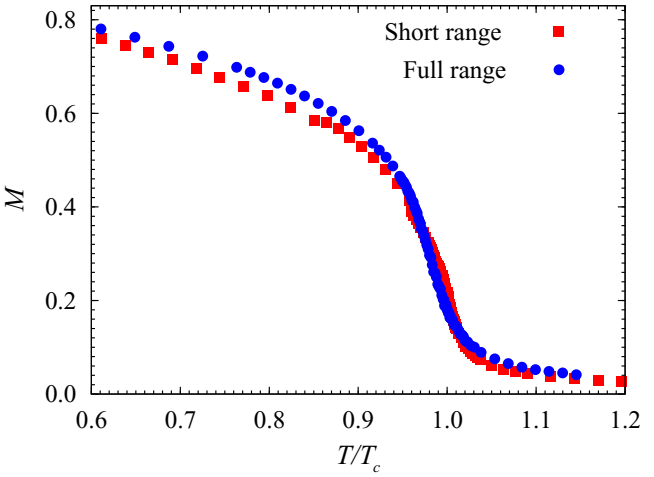

FIG. 9. Plots of M vs T/T_c for the present model and its nearest-neighbor counterpart [16]. Blue circles, present full-range model; red squares, nearest-neighbor counterpart. Both here and in Fig. 10, the plotted simulation results were obtained for $L = 24$.

this temperature value is in reasonable agreement with T_c as independently estimated via the above FSS treatment.

Let us recall that, by construction, the quantity ϕ should be size-independent at the critical temperature and thus all curves should coincide there, as is the case for the Binder cumulant. A FSS analysis was carried out and found to support this conjecture, giving results consistent with those for U_L.

To summarize, we propose for the critical temperature the value $T_c = 0.655 \pm 0.005$ versus the corresponding value 1.877 ± 0.001 in Ref. [16], thus the ratio $\rho = T_c/|W_{GS}|$ drops to roughly one-half of its short-range counterpart ($\approx$0.24 versus $\approx$0.470), and this suggests that the long-range tail of the interaction reduces the stability range of the ordered phase in comparison with the nearest-neighbor case. Comparison with the short-range counterpart was also realized in Figs. 9 and 10, where simulation results for M and $\overline{P}_2$, obtained with the largest sample size used in both studies ($L = 24$), are plotted versus T/T_c; the figures show a pronounced similarity, as well as a mild but recognizable strengthening of orientational order in the low-temperature region.

On the other hand, the critical behavior was found to be governed by the critical exponents $\nu = 0.69 \pm 0.08$, $\beta = 0.38 \pm 0.03$, and $\alpha = 0.13 \pm 0.02$. Except for the above result $\gamma = 1.31 \pm 0.05$, these values are in agreement with previous renormalization-group (RG) calculations for isotropic dipolar criticality (Table I in Ref. [6]), as well as the experimental measurements of Ref. [5] on $Cr_{70}Fe_{30}$, obtained on films of appropriate thickness. Since the value of γ is highly affected by large fluctuations in the critical region, in order to get a meaningful result we employed the hyperscaling relations to obtain $\gamma \approx 1.37$. Thus the model investigated here is consistent with the isotropic dipolar universality class; comparison between transitional properties for the present

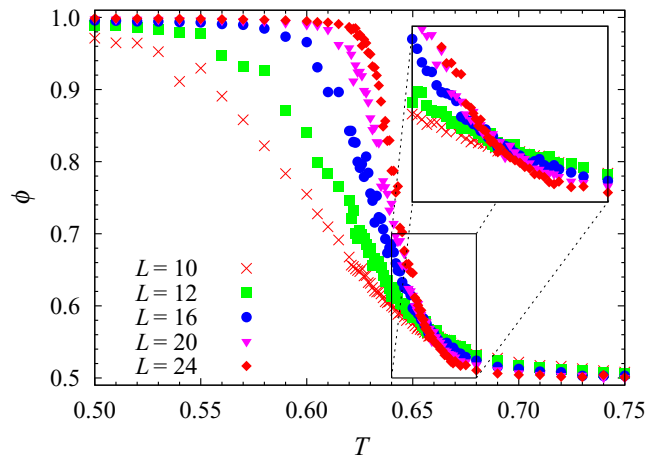

FIG. 8. Simulation results for the quantity ϕ, as defined in the text [Eq. (15)], obtained with different sample sizes; same meaning of symbols as in Fig. 1.

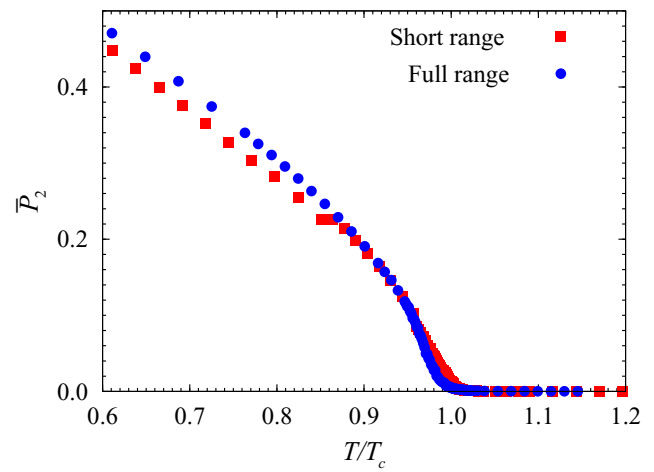

FIG. 10. Plots of $\overline{P}_2$ vs T/T_c for the present model and its nearest-neighbor counterpart [16]; same meaning of symbols as in Fig. 9.

TABLE I. Comparison between transitional properties for the present model and its nearest-neighbor counterpart [16].

	Present model	Ref. [16]
W_{GS}	-2.676	-4
T_c	0.655 ± 0.005	1.877 ± 0.001
$\rho = \frac{T_c}{\lvert W_{GS}\rvert}$	≈ 0.24	≈ 0.470
α	0.13 ± 0.02	0.13 ± 0.02
β	0.38 ± 0.03	0.358 ± 0.006
γ	≈ 1.37	1.4 ± 0.1
ν	0.69 ± 0.08	0.713 ± 0.001

model and for its nearest-neighbor counterpart is summarized in Table I.

As for comparison with other treatments, let us first mention that a Weiss-type molecular field approach predicts a transition temperature $T_{c,\mathrm{MF}} = \frac{2}{3}\lvert W_{GS}\rvert$, i.e., $\frac{8}{3} \approx 2.667$ for the nearest-neighbor counterpart and 1.784 in the present case [19,23], hence the ratio $T_c/T_{c,\mathrm{MF}} = \frac{3}{2}\rho$ has dropped by the same numerical factor (nearly 2) as above.

Both the nearest-neighbor and full-ranged cases of the model investigated here were studied some 60 years ago using the spherical model (SM) approach [44–48]; as for the nearest-neighbor case, the estimated transition temperature can be obtained from Eq. (32) in [46] by evaluating a multiple integral numerically, i.e., $T_{c,\mathrm{SM}} = 1.693$. In the full-ranged case, as far as we could check, Ref. [45] did not report any explicit numerical estimate of the transition temperature in their Eq. (6.1); on the other hand, some results are available in Ref. [48], via their Eq. (1.3) (with their α set to 0) and following treatment (see also their Figs. 1 and 2); these results read $F(\lambda_M) \approx 0.73$, and hence $T_{c,\mathrm{SM}} \approx 0.457$.

The critical exponents reported in the above papers were $\beta = \frac{1}{2}$ and $\alpha = 0$ for both cases: in both cases, the configurational specific heat C_V/k_B was found to remain constant at $\frac{3}{2}$ for $T \leqslant T_{c,\mathrm{SM}}$, and to change continuously but with a discontinuous slope at $T = T_{c,\mathrm{SM}}$.

An interaction model defined by an extension of (1) was later studied in [49] by RG; the interaction potential was defined by

$$W_{ij} = \epsilon[-(1+2\sigma)(3+2\sigma)(\mathbf{u}_i \cdot \hat{\mathbf{r}}_{ij})(\mathbf{u}_j \cdot \hat{\mathbf{r}}_{ij}) + (1+2\sigma)(\mathbf{u}_i \cdot \mathbf{u}_j)]/r^{3+\sigma}, \tag{18}$$

where $\sigma \geqslant 0$ is a real parameter: all critical exponents with the exception of β were found to depend on σ, and the limiting case $\sigma = 0$ corresponded to the model studied here, for which Eqs. (47) in the named paper [49] yield $\alpha = 1$, $\beta = \frac{1}{2}$, $\nu = 1$, $\eta = 2$, and $\gamma = 0$.

V. CONCLUSIONS

We have studied here the transitional behavior resulting from the full-ranged counterpart of the lattice-spin model in Refs. [16,25] by means of simulation as well as a detailed analysis of the results. FSS basically suggests a universality class with critical exponents $\nu = 0.69 \pm 0.08$, $\beta = 0.38 \pm 0.03$, and $\alpha = 0.13 \pm 0.02$, and a critical temperature $T_c = 0.655 \pm 0.005$, i.e., consistent with an isotropic dipolar critical point [5,6] and different from the nearest-neighbor ferromagnetic Heisenberg one. Analysis of second-rank properties has revealed the existence of secondary nematic order, destroyed by ground-state degeneracy but restored in the low-temperature phase, through a mechanism of order by disorder (see Ref. [16] and others quoted therein).

The ratio $\rho = T_c/\lvert W_{GS}\rvert$ drops to roughly one-half of its short-range counterpart (≈ 0.24 versus ≈ 0.470), and this suggests that the long-range tail of the interaction reduces the stability range of the ordered phase in comparison with the nearest-neighbor case.

ACKNOWLEDGMENTS

The present extensive calculations were carried out on, among other machines, workstations belonging to the Sezione di Pavia of Istituto Nazionale di Fisica Nucleare (INFN); allocations of computer time by the Computer Centre of Pavia University and CILEA (Consorzio Interuniversitario Lombardo per l'Elaborazione Automatica, Segrate–Milan), as well as by CINECA (Centro Interuniversitario Nord-Est di Calcolo Automatico, Casalecchio di Reno–Bologna) and CASPUR (Consorzio interuniversitario per le Applicazioni di Supercalcolo per Università e Ricerca, Rome), are gratefully acknowledged.

APPENDIX: NEMATIC SECOND- AND FOURTH-RANK ORDER PARAMETERS

Both second- and fourth-rank nematic order parameters [26–28] were calculated by analyzing one configuration every cycle; in other words, for a generic examined configuration, the Q tensor is defined by the appropriate generalization of Eq. (11), now involving all the spins in the sample, i.e.,

$$Q_{\iota\kappa} = \tfrac{1}{2}(3F_{\iota\kappa} - \delta_{\iota\kappa}), \tag{A1}$$

with

$$F_{\iota\kappa} = \langle u_\iota u_\kappa \rangle_{\mathrm{loc}} = \frac{1}{N}\sum_{j=1}^{N}(u_{j,\iota}u_{j,\kappa}), \tag{A2}$$

where $\langle \cdots \rangle_{\mathrm{loc}}$ denotes the average over the current configuration. The fourth-rank order parameter was determined via the analogous quantity [50]

$$B_{\iota\kappa\lambda\mu} = \tfrac{1}{8}[35G_{\iota\kappa\lambda\mu} - 5(\delta_{\iota\kappa}F_{\lambda\mu} + \delta_{\iota\lambda}F_{\kappa\mu} + \delta_{\iota\mu}F_{\kappa\lambda} + \delta_{\kappa\lambda}F_{\iota\mu} + \delta_{\kappa\lambda}F_{\iota\mu} + \delta_{\lambda\mu}F_{\iota\kappa}) + (\delta_{\iota\kappa}\delta_{\lambda\mu} + \delta_{\iota\lambda}\delta_{\kappa\mu} + \delta_{\iota\mu}\delta_{\kappa\lambda})], \tag{A3}$$

where

$$G_{\iota\kappa\lambda\mu} = \langle u_\iota u_\kappa u_\lambda u_\mu \rangle_{\mathrm{loc}} = \frac{1}{N}\sum_{j=1}^{N} u_{j,\iota}u_{j,\kappa}u_{j,\lambda}u_{j,\mu}. \tag{A4}$$

The calculated tensor Q was diagonalized; let ω_k denote its three eigenvalues, and let $\mathbf{v}_k$ denote the corresponding eigenvectors. The eigenvalue with the largest magnitude (usually a positive number, thus the maximum eigenvalue) can be identified, and its average over the simulation chain defines the nematic second-rank order parameter $\overline{P}_2$. The corresponding eigenvector defines the local (fluctuating or

"instantaneous") configuration director **n** [26–28], evolving along the simulation. Moreover, a suitable reordering of eigenvalues (and hence of the corresponding eigenvectors) is needed to evaluate $\overline{P}_4$; let the eigenvalues ω_k be reordered (permuted according to some rule) to yield the values ω'_k. The procedure used here as well as in other previous papers (e.g. Refs. [51,52]) involves a permutation such that

$$|\omega'_3| \geqslant |\omega'_1|, \quad |\omega'_3| \geqslant |\omega'_2|; \tag{A5a}$$

actually there exist two such possible permutations, an odd and an even one; we consistently chose permutations of the same parity (say even ones; see also below) for all examined configurations. Recall that eigenvalue reordering also induces the corresponding permutation of the associated eigenvectors. Notice also that, in most cases, $\omega'_3 > 0$, so that the condition in Eq. (A5a) reduces to

$$\omega'_3 \geqslant \omega'_1, \quad \omega'_3 \geqslant \omega'_2; \tag{A5b}$$

this latter procedure was considered in earlier treatments of the method. As already mentioned, the second-rank order parameter $\overline{P}_2$ is defined by the average of ω'_3 over the simulation chain; on the other hand, the quantity $(\omega'_2 - \omega'_1)$, and hence its average over the chain, measure possible phase biaxiality, found here to be zero within statistical errors, as it should. The procedure outlined here was previously used elsewhere [51–56], in cases in which some amount of biaxial order might exist; the consistent choice of permutations of the same parity was found to avoid both artificially enforcing a spurious phase biaxiality (as would result by imposing an additional condition such as $|\omega'_1| \leqslant |\omega'_2|$), and artificially reducing or even quenching it (as would result by ordering ω'_1 and ω'_2 at random).

The fourth-rank order parameter was evaluated from the B tensor in the following way [50]: for each analyzed configuration, the suitably reordered eigenvectors of Q define the director frame and build the column vectors of an orthogonal matrix R, in turn employed for transforming B to the director frame; the diagonal element B'_{3333} of the transformed tensor was averaged over the production run, and identified with $\overline{P}_4$.

[1] Both electrostatic and magnetostatic dipolar interactions have the same mathematical structure (within numerical factors and usage of different units or symbols), and both interpretations are currently used in the literature; in the following, we shall be using the magnetic language.

[2] K. De'Bell, A. B. MacIsaac, and J. P. Whitehead, Dipolar effects in magnetic thin films and quasi-two-dimensional systems, Rev. Mod. Phys. **72**, 225 (2000).

[3] S. N. Kaul, Critical behaviour of Heisenberg ferromagnets with dipolar interactions and uniaxial anisotropy, in *Local-Moment Ferromagnets*, edited by M. Donath and W. Nolting, Lecture Notes in Physics Vol. 678 (Springer-Verlag, Berlin, 2005), pp. 9–29.

[4] P. M. Shand, J. G. Bohnet, J. Goertzen, J. E. Shield, D. Schmitter, G. Shelburne, and D. L. Leslie-Pelecky, Magnetic behavior of melt-spun gadolinium, Phys. Rev. B **77**, 184415 (2008).

[5] B. R. Kumar and S. N. Kaul, Magnetic order-disorder phase transition in $Cr_{70}Fe_{30}$ thin films, J. Alloys Compd. **652**, 479 (2015).

[6] A. D. Bruce and A. Aharony, Critical exponents of ferromagnets with dipolar interactions: Second-order ϵ expansion, Phys. Rev. B **10**, 2078 (1974).

[7] E. Frey and F. Schwabl, Renormalized field theory for the static crossover in isotropic dipolar ferromagnets, Phys. Rev. B **43**, 833 (1991).

[8] K. Ried, Y. Millev, M. Fähnle, and H. Kronmüller, Phase transitions in ferromagnets with dipolar interactions and uniaxial anisotropy, Phys. Rev. B **51**, 15229 (1995).

[9] E. Meloche, J. I. Mercer, J. P. Whitehead, T. M. Nguyen, and M. L. Plumer, Dipole-exchange spin waves in magnetic thin films at zero and finite temperature: Theory and simulations, Phys. Rev. B **83**, 174425 (2011).

[10] L. A. S. Mól and B. V. Costa, The phase transition in the anisotropic Heisenberg model with long range dipolar interactions, J. Magn. Magn. Mater. **353**, 11 (2014).

[11] G. M. Wysin, A. R. Pereira, W. A. Moura-Melo, and C. I. L. de Araujo, Order and thermalized dynamics in Heisenberg-like square and Kagomé spin ices, J. Phys.: Condens. Matter **27**, 076004 (2015).

[12] P. I. Belobrov, R. S. Gekht, and V. A. Ignatchenko, Ground state in systems with dipole interaction, Zh. Eksp. Teor. Fiz. **84**, 1097 (1983) [Sov. Phys. JETP **57**, 636 (1983)].

[13] M. H. Cohen and F. Keffer, Dipolar ferromagnetism at 0 K, Phys. Rev. **99**, 1135 (1955).

[14] D. E. Sullivan, J. M. Deutch, and G. Stell, Thermodynamics of polar lattices, Mol. Phys **28**, 1359 (1974).

[15] D. J. Adams and I. R. McDonald, Thermodynamic and dielectric properties of polar lattices, Mol. Phys **32**, 931 (1976).

[16] H. Chamati and S. Romano, Nematic order by thermal disorder in a three-dimensional lattice-spin model with dipolar-like interactions, Phys. Rev. E **90**, 022506 (2014).

[17] J. Schönke, T. M. Schneider, and I. Rehberg, Infinite geometric frustration in a cubic dipole cluster, Phys. Rev. B **91**, 020410 (2015).

[18] M. S. Holden, M. L. Plumer, I. Saika-Voivod, and B. W. Southern, Monte Carlo simulations of a kagome lattice with magnetic dipolar interactions, Phys. Rev. B **91**, 224425 (2015).

[19] D. C. Johnston, Magnetic dipole interactions in crystals, Phys. Rev. B **93**, 014421 (2016).

[20] A. Giuliani, Long range order for lattice dipoles, J. Stat. Phys. **134**, 1059 (2009).

[21] J. Fröhlich and T. Spencer, On the statistical mechanics of classical coulomb and dipole gases, J. Stat. Phys. **24**, 617 (1981).

[22] J. Fröhlich, R. Israel, E. H. Lieb, and B. Simon, Phase transitions and reflection positivity. I. General theory and long range lattice models, Commun. Math. Phys. **62**, 1 (1978).

[23] S. Romano, Computer simulation study of a simple-cubic dipolar lattice, Nuovo Cimento D **7**, 717 (1986).

[24] S. Romano, Computer simulation study of the singlet orientational distribution function for a model antiferroelectric nematic, Europhys. Lett. **2**, 431 (1986).

[25] S. Romano, Computer-simulation study of a three-dimensional lattice-spin model with dipolar-type interactions, Phys. Rev. B **49**, 12287 (1994).

[26] C. Zannoni, Distribution function and order parameters, in *The Molecular Physics of Liquid Crystals*, edited by G. R Luckhurst and G. W Gray (Academic Press, London, 1979), Chap. 3, p. 51.

[27] C. Zannoni, Computer simulations, in *The Molecular Physics of Liquid Crystals*, edited by G. R Luckhurst and G. W Gray (Academic Press, London, 1979), Chap. 9, p. 191.

[28] C. Zannoni, Liquid crystal observables: Static and dynamic properties, in *Advances in the Computer Simulations of Liquid Crystals*, edited by P. Pasini and C. Zannoni, NATO Science Series No. 545 (Springer, Dordrecht, 2000), p. 17.

[29] J. Villain, R. Bidaux, J.-P. Carton, and R. Conte, Order as an effect of disorder, J. Phys. **41**, 1263 (1980).

[30] C. L. Henley, Ordering Due to Disorder in a Frustrated Vector Antiferromagnet, Phys. Rev. Lett. **62**, 2056 (1989).

[31] S. Prakash and C. L. Henley, Ordering due to disorder in dipolar magnets on two-dimensional lattices, Phys. Rev. B **42**, 6574 (1990).

[32] S. Romano, Computer simulation study of a two-dimensional lattice spin model with interactions of dipolar type, Phys. Scr. **50**, 326 (1994).

[33] C. Yamaguchi and Y. Okabe, Three-dimensional antiferromagnetic q-state Potts models: Application of the Wang-Landau algorithm, J. Phys. A **34**, 8781 (2001).

[34] S. Romano and G. De Matteis, Orientationally ordered phase produced by fully antinematic interactions: A simulation study, Phys. Rev. E **84**, 011703 (2011).

[35] M. Biskup, L. Chayes, and S. A. Kivelson, Order by disorder, without order, in a two-dimensional spin system with O(2) symmetry, Ann. Henri Poincaré **5**, 1181 (2004).

[36] M. P. Allen and D. J. Tildesley, *Computer Simulation of Liquids* (Oxford University Press, Oxford, 1989).

[37] D. Frenkel and B. Smit, *Understanding Molecular Simulation From Algorithms to Applications* (Academic Press, San Diego, 1996).

[38] J. A. Barker and R. O. Watts, Structure of water: A Monte Carlo calculation, Chem. Phys. Lett. **3**, 144 (1969).

[39] Th. T. A. Paauw, A. Compagner, and D. Bedeaux, Monte-Carlo calculation for the classical F.C.C. Heisenberg ferromagnet, Physica A **79**, 1 (1975).

[40] P. Peczak, A. M. Ferrenberg, and D. P. Landau, High accuracy Monte Carlo study of the three-dimensional classical Heisenberg ferromagnet, Phys. Rev. B **43**, 6087 (1991).

[41] K. Binder, Finite size scaling analysis of Ising model block distribution functions, Z. Phys. B **43**, 119 (1981).

[42] O. Melchert, autoScale.py—A program for automatic finite-size scaling analyses: A user's guide, arXiv:0910.5403 [physics.comp-ph].

[43] H. Chamati and N. S. Tonchev, Critical behavior of systems with long-range interaction in restricted geometry, Mod. Phys. Lett. B **17**, 1187 (2003).

[44] T. H. Berlin and M Kac, The spherical model of a ferromagnet, Phys. Rev. **86**, 821 (1952).

[45] M. Lax, Dipoles on a lattice: The spherical model, J. Chem. Phys. **20**, 1351 (1952).

[46] T. H. Berlin and J. S. Thomsen, Dipole-dipole interaction in simple lattices, J. Chem. Phys. **20**, 1368 (1952).

[47] R. Rosenberg and M. Lax, High temperature susceptibility of permanent dipole lattices, J. Chem. Phys. **21**, 424 (1953).

[48] R. A. Toupin and M. Lax, Lattice of partly permanent dipoles, J. Chem. Phys. **27**, 458 (1957).

[49] S. Fakioğlu, Renormalization group and critical exponents for classical Heisenberg ferromagnet with dipole-dipole interactions, Phys. Status Solidi B **98**, 307 (1980).

[50] C. Chiccoli, P. Pasini, F. Biscarini, and C. Zannoni, The P_4 model and its orientational phase transition, Mol. Phys. **65**, 1505 (1988).

[51] R. Hashim, G. R. Luckhurst, F. Prata, and S. Romano, Computer simulation studies of anisotropic systems. XXII. An equimolar mixture of rods and discs: A biaxial nematic? Liq. Cryst. **15**, 283 (1993).

[52] S. Romano, Computer simulation study of a three-dimensional lattice spin model with anti-nematic interactions, Int. J. Mod. Phys. B **08**, 3389 (1994).

[53] S. Romano, Computer simulation study of a two-dimensional nematogenic lattice model based on the Gruhn-Hess interaction potential, Phys. Lett. A **302**, 203 (2002).

[54] S. Romano, Computer simulation study of a two-dimensional nematogenic lattice model based on the Nehring-Saupe interaction potential, Phys. Lett. A **305**, 196 (2002).

[55] S. Romano, Computer simulation study of two-dimensional nematogenic lattice models based on dispersion interactions, Physica A **322**, 432 (2003).

[56] S Romano, Computer simulation study of a two-dimensional nematogenic lattice model based on a mapping from elastic free-energy density, Phys. Lett. A **310**, 465 (2003).